PHYSICAL REVIEW B **83**, 214112 (2011)

High-pressure Raman spectroscopy and lattice-dynamics calculations on scintillating $MgWO_4$: Comparison with isomorphic compounds

J. Ruiz-Fuertes,[1,*] D. Errandonea,[1] S. López-Moreno,[2] J. González,[3,4] O. Gomis,[5] R. Vilaplana,[5] F. J. Manjón,[6] A. Muñoz,[2] P. Rodríguez-Hernández,[2] A. Friedrich,[7] I. A. Tupitsyna,[8] and L. L. Nagornaya[8]

[1]*Departamento de Física Aplicada-ICMUV, MALTA Consolider Team, Universitat de València, Edificio de Investigación, c/Dr. Moliner 50, 46100 Burjassot, Spain*

[2]*Departamento de Física Fundamental II, MALTA Consolider Team, Instituto de Materiales y Nanotecnología, Universidad de La Laguna, La Laguna, 38205 Tenerife, Spain*

[3]*DCITIMAC, MALTA Consolider Team, Universidad de Cantabria, Avda. de Los Castros s/n, 39005 Santander, Spain*

[4]*Centro de Estudios de Semiconductores, Universidad de los Andes, Mérida 5201, Venezuela*

[5]*Centro de Tecnologías Físicas: Acústica, Materiales y Astrofísica, MALTA Consolider Team, Universitat Politècnica de València, Camino de Vera s/n, 46022 Valencia, Spain*

[6]*Instituto de Diseño para la Fabricación y Producción Automatizada, MALTA Consolider Team, Universitat Politècnica de València, Camino de Vera s/n, 46022 Valencia, Spain*

[7]*Institut für Geowissenschaften, Abt. Kristallographie, Goethe-Universität Frankfurt, D-60438 Frankfurt am Main, Germany*

[8]*Institute for Scintillation Materials, UA-61001 Kharkov, Ukraine*

(Received 22 March 2011; revised manuscript received 9 May 2011; published 30 June 2011)

Raman scattering measurements and lattice-dynamics calculations were performed on magnesium tungstate ($MgWO_4$) under high pressure up to 41 GPa. Experiments were carried out on a selection of pressure media. The influence of nonhydrostaticity on the structural properties of $MgWO_4$ and isomorphic compounds is examined. Under quasihydrostatic conditions, a phase transition was found at 26 GPa in $MgWO_4$. The high-pressure phase is tentatively assigned to a triclinic structure similar to that of $CuWO_4$. We also report and discuss the Raman symmetries, frequencies, and pressure coefficients in the low- and high-pressure phases. In addition, the Raman frequencies for different wolframites are compared and the variation of the mode frequency with the reduced mass across the family is investigated. Finally, the accuracy of theoretical calculations is systematically discussed for $MgWO_4$, $MnWO_4$, $FeWO_4$, $CoWO_4$, $NiWO_4$, $ZnWO_4$, and $CdWO_4$.

DOI: 10.1103/PhysRevB.83.214112 PACS number(s): 62.50.−p, 63.20.D−, 78.30.−j

I. INTRODUCTION

Divalent-metal tungstates (AWO_4) are being studied with great interest because of their use as materials for scintillator detectors and laser-host crystals, as well as in acoustic and optical fiber applications.[1,2] Magnesium tungstate ($MgWO_4$), the mineral hunzalaite, is part of this family. With a band gap of 3.92 eV,[3] it is one of the most extensively studied metal tungstates because of its interest as a scintillator material for cryogenic applications used in the search for rare events in particle physics.[4] $MgWO_4$ crystallizes in a monoclinic structure isomorphic to wolframite, like other tungstates such as $MnWO_4$, $FeWO_4$, $CoWO_4$, $NiWO_4$, $ZnWO_4$, and $CdWO_4$. It belongs to space group $P2/c$ (SG: 12) and has a C_{2h} point-group symmetry. The structure consists of layers of alternating AO_6 (A = Mg, Mn, Fe, Co, Ni, Zn, and Cd) and WO_6 octahedral units that share edges, forming a zigzag chain[5] and creating a close-packed structure. The crystalline structure is illustrated in Fig. 1.

Several studies of the physical properties of $MgWO_4$ have been carried out at ambient pressure. In particular, the electronic, vibrational, and scintillating properties have been studied.[3,4,6] High-pressure (HP) research has proved an efficient tool for improving understanding of the main physical properties of compounds related to $MgWO_4$. However, only a limited number of HP studies have been performed on this compound. After the single-crystal x-ray diffraction (SXRD) work of Macavei and Schulz,[7] where three wolframites were studied up to 9 GPa, a few papers have appeared on the HP vibrational[8–10] and structural[6,10,11] properties of $MgWO_4$ and other wolframites. The HP behavior of $MgWO_4$ was expected to be similar to that of $ZnWO_4$, which shows only one structural phase transition at 30.6 GPa, according to Raman experiment and *ab initio* calculations.[8] However, powder x-ray diffraction (PXRD) experiments carried out on both $MgWO_4$ and $ZnWO_4$ showed that these wolframites undergo, in addition to the expected phase transition around 31 GPa, a phase transition around 17 GPa.[6] From combined Raman spectroscopic and *ab initio* calculations,[8,9] it has been established that the monoclinic β-fergusonite structure (space group $C2/c$, SG: 13) could be the most probable HP phase for these compounds. In addition, a triclinic structure (space group $P\bar{1}$, SG: 2) similar to that of $CuWO_4$ is energetically competitive with the wolframite and β-fergusonite phases. This fact has been used to explain the additional phase transition observed by means of PXRD in $MgWO_4$ and $ZnWO_4$.

To further understand and explain the structural behavior of wolframites under compression, we performed a combined Raman spectroscopy and theoretical study of $MgWO_4$ up to 41 GPa. Experiments were carried out using various pressure-transmitting media (PTM), including neon, methanol-ethanol, spectroscopic paraffin, and no PTM. This study provides us not only with better knowledge about $MgWO_4$ vibrational properties but also with the possibility of correlating the general trends of wolframites at HP.

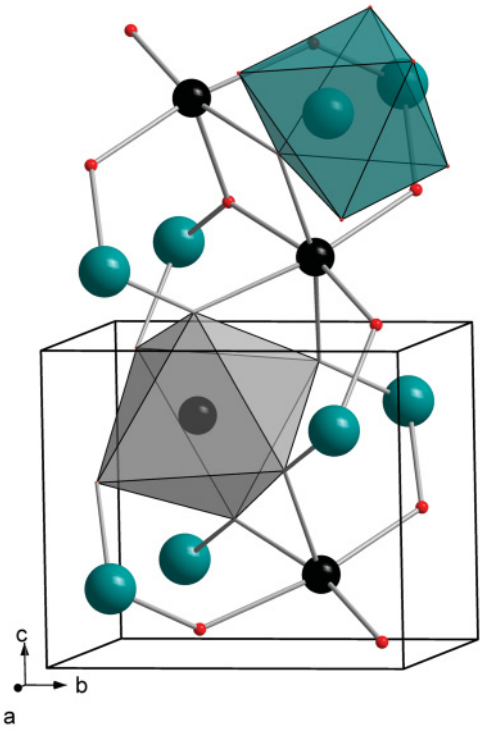

FIG. 1. (Color online) $MgWO_4$ wolframite. Big spheres are W atoms, middle-sized ones are Mg atoms, and small ones are O atoms.

II. EXPERIMENTAL DETAILS

Five series of Raman measurements were performed on 10-μm-thick platelets cleaved from $MgWO_4$ single crystals (or with micron-sized powders grounded from the crystals) using three Raman spectrometers in backscattering geometry. Single crystals were prepared using the flux growth technique developed at the Institute for Scintillation Materials (Kharkov, Ukraine).[12] A stoichiometric mixture of MgO and WO_3 (99.99%) was added to the flux prepared from Na_2WO_4 (99.95%) at 790 °C in a platinum crucible. Single-crystalline samples of $MgWO_4$ crystals of $\sim$1 cm^3 were grown by pulling the seed from the melted flux solution.

The first experiment was carried out using a Renishaw Raman spectrometer (RM-1000) that had a 1800 grooves/mm grating and 100-μm slit and was equipped with a HeNe laser (633 nm, 50 mW), a 20× objective (1 cm^{-1} of spectral resolution) and a nitrogen (N_2)-cooled charge-coupled device (CCD) detector. The sample was loaded in a Boehler-Almax diamond-anvil cell (DAC) with neon as the pressure medium, and a maximum pressure of 40 GPa was reached. The second and third experiments were carried out using a LabRam high-resolution ultraviolet microRaman spectrometer with a 1200 grooves/mm grating, a 100-μm slit, and a 50× objective (spectral resolution of 2 cm^{-1}), in combination with a thermoelectric-cooled multichannel CCD detector. A 532.12-nm laser line with a power of 10 mW was used. In the second and third experiments, we went up to 41 GPa (31 GPa) and used a Boehler-Almax (membrane type) DAC loaded with neon (no PTM). $MgWO_4$ in powder form was used in the third experiment (no PTM). The fourth and fifth experiments were carried out using a triple monochromator Jobin-Yvon T64000 in the subtractive mode that had a resolution of 0.8 cm^{-1}, a 1800 grooves/mm grating, and a 100-μm slit and was equipped with a liquid N_2-cooled CCD detector. A 514.5-nm line of an argon laser was focused down with a 20× objective and kept the power on the sample below 5 mW to avoid laser-heating effects on the probed material and the concomitant softening of the observed Raman peaks. In the fourth experiment, pressure was increased to 21 GPa in a membrane-type DAC using a 4:1 mixture of methanol-ethanol as PTM; in the fifth experiment, we went up to 30 GPa using $MgWO_4$ powder with purity higher than 99.5% (Mateck), a membrane DAC, and a spectroscopic paraffin as PTM. In all experiments, pressure was determined using the ruby-fluorescence technique[13] (with $\pm$1% maximum uncertainty). In addition, we collected Raman spectra of $NiWO_4$, $CoWO_4$, and $FeWO_4$ at ambient pressure to compare them with theoretical calculations. Powders of 99.9% purity (Alfa Aesar) were used in the experiments.

III. CALCULATIONS DETAILS

In recent years, *ab initio* methods have allowed detailed studies of the energetics of materials under HPs.[14] For this paper, total-energy calculations were done within the framework of the density-functional theory (DFT). The Kohn-Sham equations were solved using the projector-augmented wave[15,16] method as implemented in the Vienna *ab initio* simulation package.[17] We used a plane-wave energy cutoff of 520 eV to ensure accurate and high precision in the calculations. The exchange and correlation energy was described within the generalized gradient approximation (GGA) in the Perdew-Burke-Ernzerhof[18] prescription for $MgWO_4$. The Monkhorst-Pack[19] grid used for Brillouin-zone (BZ) integrations ensured highly converged results for the analyzed structures (to about 1 meV per formula unit). Different studies of transition metal compounds have pointed out that GGA often yields incorrect results for systems with high correlated electrons. The implementation of the DFT+U method has been found to have some influence on transition metal compounds.[20] The GGA+U method was used to account for the strong correlation between the electrons in the d orbitals on the basis of Dudarev's method[20] for the study of AWO_4 (A = Mn, Co, Ni, and Fe). In this method, the on-site Coulomb interaction, Hubbard term U, and on-site exchange interaction J_H are treated together as $U_{\text{eff}} = U - J_H$. For our GGA+U calculations, we chose U_{eff} = 3.9, 4.2, 4.3, and 7 eV for Mn, Co, Ni, and Fe atoms, respectively. We performed spin density calculations for these compounds and found that the antiferromagnetic configuration was the stable one for Mn, Co, Ni, and Fe wolframites. In the relaxed equilibrium configuration, the forces are $<$6 meV/Å per atom in each of the Cartesian directions. Lattice-dynamics calculations of phonon modes were performed at the zone center (Γ point) of the BZ. The calculations provided information about the frequency, symmetry and polarization vector of the vibrational modes in each structure. Highly converged results on forces are required for the calculation of the dynamical matrix from lattice-dynamics calculations. We used the direct force-constant approach (or supercell method).[21] The construction

of the dynamical matrix at the point of the BZ is particularly simple and involves separate calculation of the forces in which a fixed displacement from the equilibrium configuration of the atoms within the primitive unit cell is considered. Symmetry further reduces the computational efforts by reducing the number of such independent displacements in the analyzed structures. Diagonalization of the dynamical matrix provides both the frequencies of the normal modes and their polarization vectors. It allows us to identify the irreducible representations and the character of phonon modes at the Γ point.

IV. RESULTS AND DISCUSSION

A. Low-pressure phase

According to group-theory analysis, the wolframite structure has 36 vibrational modes, 18 of which are Raman active (even vibrations g) and 18 of which are infrared active (odd vibrations u) at the Γ point: $\Gamma = 8A_g + 10B_g + 8A_u + 10B_u$. The assignment of the modes is shown in Table I.[6] It has been argued that for wolframite-type AWO_4 compounds the Raman modes can be classified as internal and external modes with respect to the WO_6 octahedra.[8,9] Thus, wolframites have up to six internal stretching modes that arise from the six W-O bonds in the WO_6 octahedra. Because W is heavier than Mg and W-O covalent bonds are stiffer than Mg-O bonds, it is reasonable to think of the material as two separated blocks, one concerning the WO_6 units and the second one concerning the Mg^{2+} cation. Moreover, the WO_6 octahedra are quite incompressible, with the MgO_6 octahedra accounting for most of the volume reduction of the structure under pressure. Consequently, the six internal stretching modes of $MgWO_4$ are in the high-frequency part of the Raman spectrum. They are the A_g modes with frequencies of 917, 713, 552, and 420 cm^{-1} and the B_g modes with frequencies of 809 and 684 cm^{-1}.

Figures 2, 3(a), and 3(b) show the Raman spectra of $MgWO_4$ at pressures up to 41.0, 30.6, and 30.2 GPa, respectively. Data were collected using different PTM: neon, no PTM, and spectroscopic paraffin, respectively. Depending upon the experiment, we can follow all Raman modes of wolframite up to 17–29 GPa when the clear appearance of an additional mode just below the most energetic one, plus the intensity drop of several of the wolframite modes, indicates the onset of a phase transition. Figure 4 shows the evolution of the measured Raman modes as obtained from the experiments with Ne and methanol-ethanol, which are in good agreement. Because the Raman modes evolve linearly with pressure, we obtained the pressure coefficients ($d\omega/dP$) by means on linear fits. HP and low pressure (LP)[6] results are summarized in Table I, together with results from *ab initio* calculations. The mode assignment stated in Table I is supported by theory and polarized Raman measurements.

Both the experimental and the calculated modes agree well; the major difference for most of them is <10 cm^{-1}. This good agreement accounts for their pressure coefficients except for that of the B_g mode at 405 cm^{-1}. For this mode, the experimental pressure coefficient is five times lower than the calculated one. From the pressure coefficients of the mode frequencies and the bulk modulus B_0, we obtained the Grüneisen parameters $\gamma = (B_0/\omega) \cdot (d\omega/dP)$, for $MgWO_4$ (Table I). For the experimental Grüneisen parameters, the value for B_0 (160 GPa) was taken from Ref. 6; for the calculated data, the theoretical value of B_0 (161 GPa) was used for self-consistency. Both the experimental and the calculated Grüneisen parameters well match each other for the LP phase, with only a mismatch shown again for the 405 cm^{-1}

TABLE I. *Ab initio* calculated and experimental (Ref. 6) Raman modes together with their pressure coefficients and Grüneisen parameters for the wolframite $P2/c$ phase of $MgWO_4$.

	Ab initio Calculation			Experiment		
Mode	ω (cm^{-1})	$d\omega/dP$ ($cm^{-1}GPa^{-1}$)	γ	ω (cm^{-1})	$d\omega/dP$ ($cm^{-1}GPa^{-1}$)	γ
B_g	104.3	0.80	1.23	97.4	0.69	0.93
A_g	152.1	0.24	0.25	155.9	0.26	0.22
B_g	184.6	0.44	0.38	185.1	0.51	0.36
B_g	215.3	0.62	0.46	215.0	0.63	0.38
B_g	267.7	1.01	0.61	266.7	1.01	0.50
A_g	287.0	0.51	0.29	277.1	0.55	0.26
A_g	301.5	1.93	1.03	294.1	1.92	0.86
B_g	308.8	1.79	0.93	313.9	1.99	0.83
A_g	361.8	4.20	1.87	351.9	3.52	1.31
B_g	372.3	3.90	1.69	384.8	4.95	1.69
B_g	405.2	5.42	2.15	405.2	1.47	0.48
A_g	411.3	1.67	0.65	420.4	1.59	0.50
B_g	523.4	3.31	1.02	518.1	3.30	0.84
A_g	560.9	3.33	0.96	551.6	3.00	0.71
B_g	683.2	4.34	1.02	683.9	4.09	0.78
A_g	720.7	3.34	0.75	713.2	3.35	0.62
B_g	809.8	4.14	0.82	808.5	3.69	0.60
A_g	912.5	3.61	0.64	916.8	3.19	0.46

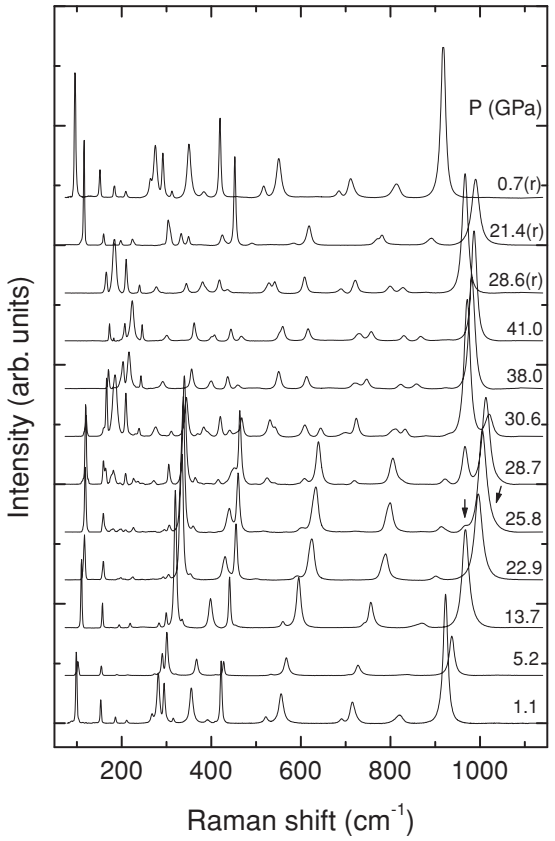

FIG. 2. Raman spectra of wolframite $MgWO_4$ at selected pressures (Ne experiment). Arrows indicate the appearance of the strongest band of the HP phase and the strongest band of the wolframite phase after the transition onset. All spectra are measured upon pressure increase with the exception of those denoted by (r), which correspond to pressure release.

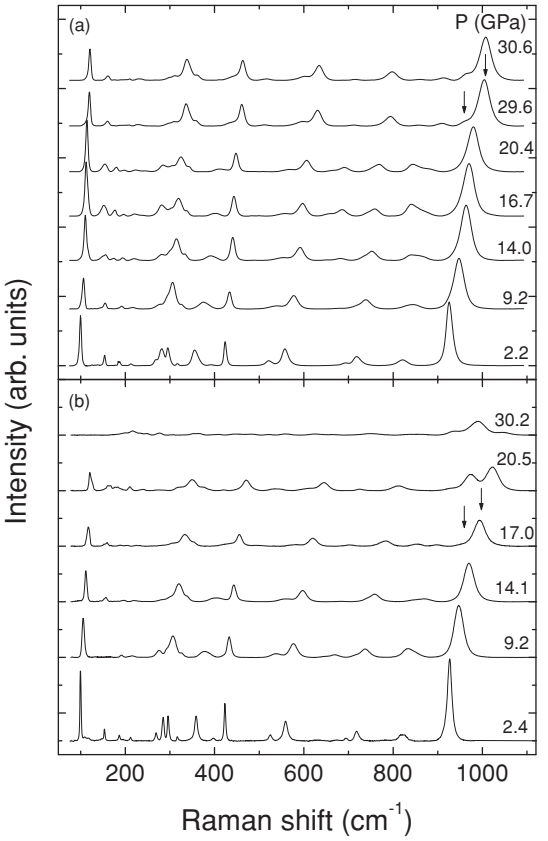

FIG. 3. Raman spectra of wolframite $MgWO_4$ at different pressures. (a) No PTM. (b) Spectroscopic paraffin. Arrows indicate the appearance of the strongest HP peak and the strongest peak of the LP phase after the transition onset.

mode. This discrepancy was not previously observed for other wolframites ($ZnWO_4$ and $CdWO_4$), and its origin remains unclear.

In all experiments, the behavior of the modes upon compression is quite similar up to 10 GPa. However, differences start to appear at higher pressures in the experiments performed without PTM or with paraffin. If no PTM is used, most modes show a faster frequency increase beyond 10 GPa than in experiments using Ne. One example is the A_g mode with the frequency 294 cm^{-1}. For only few modes, like the 420 cm^{-1} A_g mode, the pressure behavior is the same in all experiments. If paraffin is used as the PTM, all modes have a larger pressure coefficient than in the rest of the experiments beyond 10 GPa. The origin of these differences can be the presence of non-negligible uniaxial stress in the experiments performed without PTM or with paraffin.[22] Consequently, these two experiments were not used to obtain the results summarized in Fig. 4 and Table I.

By means of the harmonic approximation, if we consider that the atoms are bonded by springs, then the frequency of the oscillations is directly proportional to the inverse square root of the reduced mass of the cations. For simplicity, we consider that our system consists of two separate blocks: the cation A and the anion WO_4. Thus, to identify some general trends on AWO_4 wolframites, we plotted the Raman shifts of the different vibrational modes of the wolframite series as a function of the inverse of the square root of the reduced mass μ of the A cation and the WO_6 polianion ($1/\mu = 1/m_A + 1/m_{WO_6}$) in Figs. 5 and 6. Table II summarizes the experimental[6,8–10,23,24] and calculated Raman modes and pressure coefficients (in parentheses) for the whole wolframite family. The first conclusion we obtained is that the seven compounds have a similar overall mode distribution. As expected, internal high-frequency modes, in which O atoms vibrate against W atoms, are close for all five compounds and show little dependence of the mass of the A^{2+} cation. On the contrary, the external low-frequency modes, which involve motions of WO_6 polyhedra against the A cation, are more sensitive to the mass of the divalent cation. In particular, we found that $MgWO_4$, $ZnWO_4$, and $CdWO_4$ follow a systematic trend and $MnWO_4$, $FeWO_4$, $CoWO_4$, and $NiWO_4$ follow another trend. As can be seen in Table II and Figs. 5 and 6, the wolframites that do not involve magnetic cations ($MgWO_4$, $ZnWO_4$, and $CdWO_4$) show an inverse proportional relationship between the frequencies of the external modes and the square root of the reduced mass μ. In particular, the B_g mode located at 405 cm^{-1} for $MgWO_4$ is extremely sensitive to the mass of the divalent cation. Indeed, Fig. 5 and Table II show that the mode-frequency (ν) sequence in the 350–400 cm^{-1} region changes from $\nu_{B_g} > \nu'_{B_g} > \nu_{A_g}$ in

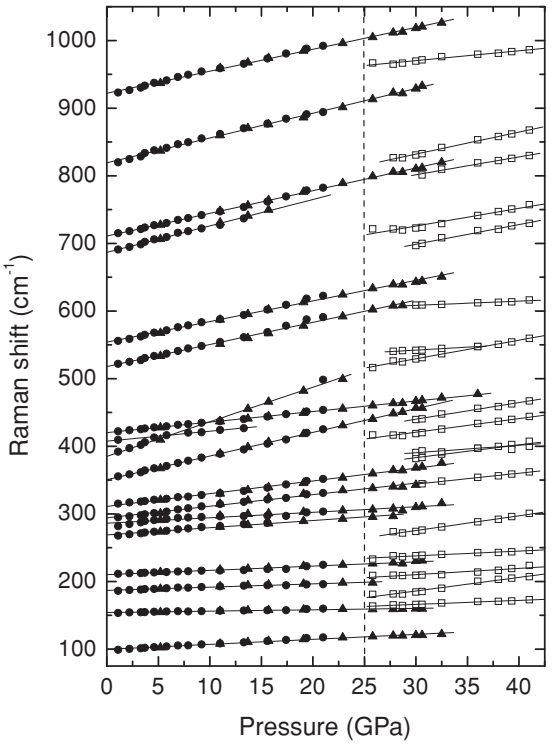

FIG. 4. Pressure dependence of the Raman mode frequencies of the wolframite (solid symbols) and HP (empty symbols) phases of $MgWO_4$ and linear fittings. Circles denote methanol-ethanol experiments, and triangles belong to Ne experiments. The vertical dashed line indicates the onset of the phase transition.

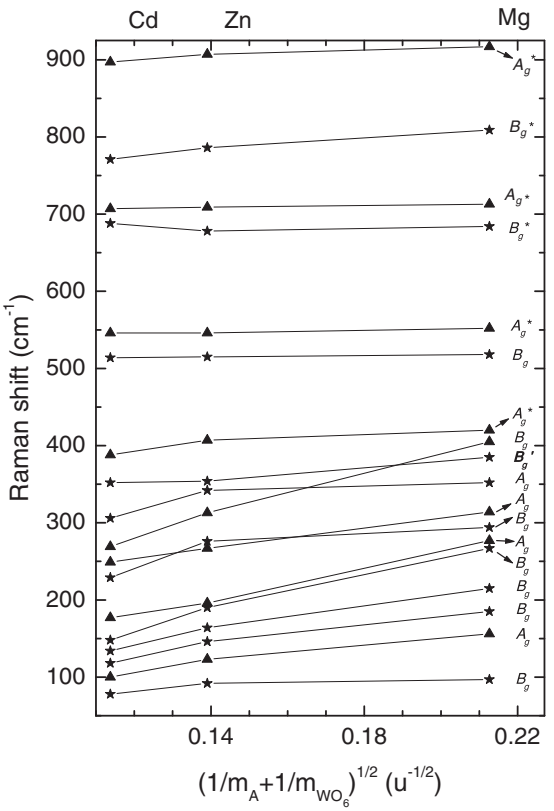

FIG. 5. Divalent-cation reduced-mass dependence of the ambient conditions Raman frequencies for $MgWO_4$, $ZnWO_4$, and $CdWO_4$. Stars indicate B_g modes, whereas the triangles refer to A_g modes. Mode symmetries are indicated, and the mode is denoted as $\boldsymbol{B}_g'$.

$MgWO_4$ to $\nu'_{B_g} > \nu_{A_g} > \nu_{B_g}$ in $CdWO_4$ (the prime symbol is used to differentiate between B_g modes). These three modes have similar pressure coefficients in the three compounds. In addition, the influence of the atomic mass of the divalent cation on the phonon frequencies of the external modes, which we observed in nonmagnetic wolframites, is similar to that found in alkaline-earth tungstates.[25] In contrast, the external-mode frequencies of $MnWO_4$, $FeWO_4$, $CoWO_4$, and $NiWO_4$ show the opposite behavior as they increase with the divalent-cation mass. This different behavior could be caused by the influence of magnetic interactions and second-order Jahn-Teller effects, which induce strong distortions of the WO_6 and AO_6 octahedra. These effects could even become strong enough to induce triclinic distortion, as is the case for $CuWO_4$.[10] The Raman spectrum of wolframite-type $CuWO_4$, which is obtained at 10 GPa after undergoing a phase transition, resembles that of magnetic wolframites (Table II).[10] This fact supports the hypothesis described earlier. Discussion of the influence of magnetic and Jahn-Teller effects on the lattice vibrations of wolframites is beyond the scope of this paper.

In the cases of $MgWO_4$, $ZnWO_4$, and $CdWO_4$, a few significant differences were observed. There is a frequency gap between the less energetic mode (97 cm^{-1}) and the following one (156 cm^{-1}) that happens to be higher for $MgWO_4$ than for the other members of the wolframite family. Furthermore, the A_g (277 cm^{-1}) mode moves more slowly with pressure than the B_g (294 cm^{-1}) mode for $MgWO_4$, whereas the opposite happens for $ZnWO_4$ and $CdWO_4$. Another difference is related to the pressure coefficient of the B_g mode located near 385 cm^{-1} for $MgWO_4$ and at 354 and 352 cm^{-1} for $ZnWO_4$ and $CdWO_4$, respectively, which is around four times higher than that of the surrounding modes. Hence, this mode crosses other modes at HPs, as can be seen in Fig. 4 as well as in Refs. 8 and 9. Finally, the pressure coefficients of the four internal modes at higher frequencies are slightly lower for $MgWO_4$ than for $ZnWO_4$ and $CdWO_4$. This observation is consistent with $MgWO_4$ being the least compressible compound among the wolframite family.

B. *Ab initio* calculations

Ab initio calculations usually describe well the HP structural properties of wolframites.[6,8,9] In particular, calculations have been performed for $MgWO_4$, $CdWO_4$, $ZnWO_4$, and $MnWO_4$. Here, we report structural calculations for $FeWO_4$, $NiWO_4$, and $CoWO_4$. For the three compounds, a wolframite-type structure is found to be the stable structure at ambient pressures. These compounds could be magnetic because of the presence of the Co^{2+}, Fe^{2+}, and Ni^{2+} cations, so we considered different magnetic configurations. We found the LP phase of the three compounds to have a wolframite structure with an antiferromagnetic configuration. In this configuration, Mn, Fe, Co, and Ni have a magnetic moment of 4.3, 3.8, 2.7, and 1.65 μB, respectively. These magnetic structures

TABLE II. Experimental (Exp.) and calculated (Calc.) Raman modes in reciprocal centimeters of all wolframite compounds. The experimental data of $MgWO_4$, $FeWO_4$, $CoWO_4$, and $NiWO_4$ are from the present study. The experimental pressure coefficients $d\omega/dP$ (cm^{-1} GPa^{-1}) are also included in parentheses for those compounds that are available. The internal modes are denoted by an asterisk.

	$MgWO_4$[6]			$MnWO_4$[23,24]		$ZnWO_4$[8]		$CdWO_4$[9]	
Mode	Exp.	Calc.	Mode	Exp.	Calc.	Exp.	Calc.	Exp.	Calc.
B_g	97.4 (0.69)	104 (0.80)	B_g	89 (0.73)	95 (0.78)	91.5 (0.95)	84 (1.02)	78 (0.52)	67 (0.89)
A_g	155.9 (0.26)	152 (0.24)	A_g	129 (0.02)	129 (−0.06)	123.1 (0.65)	119 (0.48)	100 (0.69)	97 (0.36)
B_g	185.1 (0.51)	185 (0.44)	B_g	160 (0.22)	165 (0.27)	145.8 (1.20)	137 (1.33)	118 (1.02)	111 (0.91)
B_g	215.0 (0.63)	215 (0.62)	B_g	166 (0.78)	171 (0.54)	164.1 (0.72)	163 (0.42)	134 (0.82)	126 (0.74)
B_g	266.7 (1.01)	268 (1.01)	B_g	177 (1.03)	183 (0.72)	189.6 (0.67)	182 (0.41)	148 (1.51)	142 (1.03)
A_g	277.1 (0.55)	287 (0.51)	A_g	206 (2.01)	226 (2.19)	196.1 (2.25)	186 (2.52)	177 (0.71)	177 (0.70)
A_g	294.1 (1.92)	302 (1.93)	B_g	272 (2.03)	278 (1.82)	267.1 (1.32)	261 (2.16)	249 (2.14)	239 (1.86)
B_g	313.9 (1.99)	309 (1.79)	A_g	258 (0.30)	264 (0.34)	276.1 (0.87)	264 (0.82)	229 (0.29)	220 (0.11)
A_g	351.9 (3.52)	362 (4.20)	B_g	294 (2.02)	296 (2.72)	313.1 (1.74)	298 (1.44)	269 (1.41)	252 (1.70)
B'_g	384.8 (4.95)	372 (4.90)	A_g	327 (1.50)	338 (2.4)	342.1 (1.74)	324 (1.70)	306 (0.04)	287 (0.12)
B_g	405.2 (1.47)	405 (5.42)	B'_g	356 (4.09)	373 (4.6)	354.1 (3.87)	342 (3.3)	352 (4.55)	338 (4.14)
A^*_g	420.4 (1.59)	411 (1.67)	A^*_g	397 (1.69)	389 (1.71)	407 (1.65)	384 (1.84)	388 (2.33)	357 (2.39)
B_g	518.1 (3.30)	523 (3.31)	B_g	512 (2.86)	509 (2.93)	514.5 (3.18)	481 (3.1)	514 (3.86)	490 (2.63)
A^*_g	551.6 (3.00)	561 (3.33)	A^*_g	545 (2.39)	548 (2.77)	545.5 (3.00)	515 (3.07)	546 (2.32)	531 (1.51)
B^*_g	683.9 (4.09)	683 (4.34)	B^*_g	674 (4.20)	662 (3.79)	677.8 (3.90)	636 (3.90)	688 (4.35)	656 (3.68)
A^*_g	713.2 (3.35)	721 (3.34)	A^*_g	698 (3.08)	694 (2.75)	708.9 (3.30)	679 (3.24)	707 (3.92)	684 (3.32)
B^*_g	808.5 (3.69)	810 (4.14)	B^*_g	774 (3.58)	775 (3.54)	786.1 (4.40)	753 (4.00)	771 (4.30)	743 (3.95)
A^*_g	916.8 (3.19)	913 (3.61)	A^*_g	885 (1.63)	858 (1.82)	906.9 (3.70)	862 (3.36)	897 (3.66)	864 (2.88)

	$FeWO_4$		$CoWO_4$		$NiWO_4$		$CuWO_4$[10]	
Mode	Exp.	Calc.	Exp.	Calc.	Exp.	Calc.	Exp.	Calc.
B_g	86	92 (1.13)	88	99 (0.63)	91	103 (0.63)	97 (0.90)	90 (0.75)
A_g	124	132 (0.22)	125	140 (0.17)	141	147 (0.11)	129 (−0.09)	111 (0.32)
B_g	154	162 (1.50)	154	168 (0.52)	165	180 (0.55)	157 (0.87)	154 (0.19)
B_g	174	179 (0.59)	182	192 (0.21)	190	207 (0.56)	178 (0.45)	173 (1.01)
B_g		184 (1.06)	199	193 (0.59)	201	220 (0.79)	190 (0.43)	186 (0.39)
A_g	208	213 (3.81)		237 (2.37)		246 (2.24)	192 (2.50)	203 (0.38)
B_g	266	263 (3.17)	271	292 (2.27)	298	305 (2.73)	275 (1.34)	215 (0.44)
A_g		278 (0.67)		299 (0.52)	298	313 (0.75)	285 (2.45)	265 (0.67)
B_g	299	295 (1.55)	315	317 (1.96)		329 (1.68)	312 (1.48)	285 (0.09)
A_g	330	330 (2.73)	332	361 (3.46)	354	382 (3.18)	316 (1.58)	315 (0.29)
B'_g		350 (4.27)		379 (3.99)		402 (3.85)	367 (3.57)	331 (0.31)
A^*_g	401	406 (0.54)	403	407 (1.15)	412	416 (1.31)	391 (1.33)	459 (1.43)
B_g	500	483 (3.47)	496	510 (2.9)	505	512 (2.99)	505 (3.30)	502 (3.57)
A^*_g	534	530 (3.48)	530	551 (3.25)	537	557 (3.33)	548 (2.97)	561 (2.57)
B^*_g	653	637 (4.77)	657	646 (3.81)	663	671 (3.85)	645 (3.74)	699 (2.78)
A^*_g	692	676 (3.75)	686	692 (3.01)	688	702 (3.07)	686 (2.99)	745 (1.77)
B^*_g	777	754 (4.50)	765	781 (3.88)	765	786 (4.08)	749 (4.04)	919 (2.12)
A^*_g	878	866 (3.68)	881	874 (2.80)	887	881 (3.17)	847 (3.09)	963 (2.53)

agree with neutron-diffraction studies and x-ray absorption experiments.[26–28] The obtained magnetic orders and moments are also comparable with results reported for antiferromagnetic $MnWO_4$.[23] In Table III, we summarize the calculated structural parameters and compare them with experimental values.[29,30] The lattice parameters and the atomic coordinates have good agreement, with an underestimation of the unit-cell volume for $CoWO_4$ and $NiWO_4$ of 4.8% and 4.2%, respectively, and an overestimation for $FeWO_4$ of 3.5%. These differences are typical for DFT calculations.[31,32]

In addition to the Raman-active phonons of $MgWO_4$, we calculated the phonons for $MnWO_4$, $FeWO_4$, $CoWO_4$, and $NiWO_4$. Table II shows that at ambient pressure the agreement of calculations with experiment is good. Raman-mode assignments were made based upon calculations. The internal modes were identified and are depicted by asterisks in the table. For $NiWO_4$, the present DFT calculations agree much better with experiments than previous calculations performed using the periodic linear combination of atomic orbitals method.[33] In particular, calculations gave excellent agreement for the internal modes; discrepancies are always

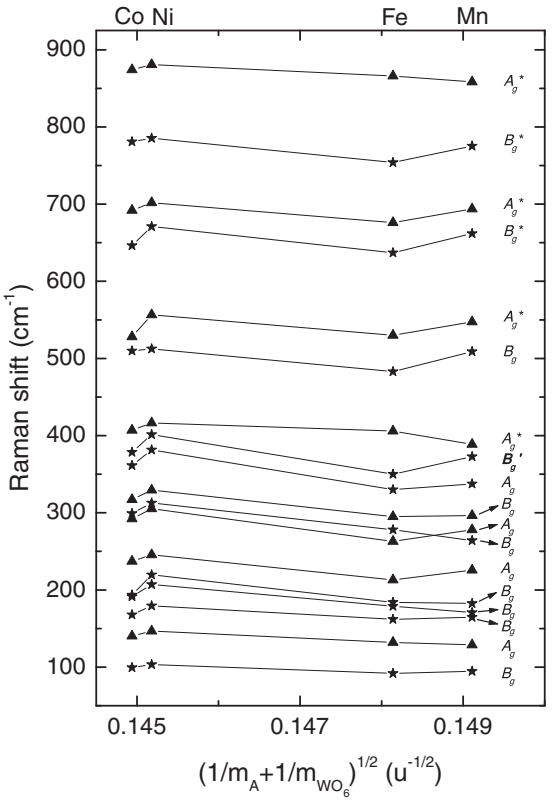

FIG. 6. Divalent-cation reduced-mass dependence of the ambient conditions Raman frequencies for $MnWO_4$, $FeWO_4$, $CoWO_4$, and $NiWO_4$. Stars indicate B_g modes, whereas the triangles refer to A_g modes. Mode symmetries are indicated, and the mode is denoted as $\boldsymbol{B}'_{\boldsymbol{g}}$.

smaller than 5%. As discussed earlier, for $MgWO_4$ the agreement is not only good for ambient pressure frequencies but also for pressure coefficients. The same can be stated for $ZnWO_4$ and $CdWO_4$.[8,9] Therefore, *ab initio* calculations proved to be an efficient tool to characterize the lattice dynamics of wolframites at ambient and HP. Only for the 405 cm^{-1} external B_g mode are the discrepancies in the pressure coefficient important. This mode is the same one that is extremely sensitive to the mass of the divalent cation, as discussed in the previous section. For $NiWO_4$, $CoWO_4$, and $FeWO_4$, no HP Raman measurements have been performed yet. Consequently, given the good description provided for other wolframites by *ab initio* calculations, we calculated the pressure evolution of Raman phonons for $MnWO_4$, $NiWO_4$, $CoWO_4$, and $FeWO_4$. Results are shown in Table II, where the pressure coefficients are included. As for other wolframites, the pressure coefficient is larger for the internal modes than for the rest of the modes. Within the internal modes, the B_g modes are those more sensitive to pressure. Also, the external modes with the highest frequencies (two B_g modes) are sensitive to pressure. On the other hand, there is a low-frequency A_g mode, with a frequency between 124 and 141 cm^{-1}, that in the three compounds has an extremely small pressure coefficient. The triclinic wolframite-type $CuWO_4$ shows a pressure evolution of the phonon frequencies similar to those of $MnWO_4$, $NiWO_4$, $CoWO_4$, and $FeWO_4$ (Table II). In contrast to scheelite-structured oxides,[25] no phonon softening occurs in wolframites upon compression.

C. High-pressure phase

As mentioned in Sect. IV.A, the occurrence of a phase transition is observed by the appearance of an additional Raman mode at a wavelength slightly smaller than the most intense mode of wolframite at pressures between 17 and 30 GPa, depending upon the PTM used (Figs. 2 and 3). The phase transition is reversible, with little hysteresis in all experiments. In the experiment performed using Ne as PTM (Fig. 2), the appearance of the new mode at 25.8 GPa is followed by a quick increase of its intensity and the appearance of extra Raman bands. A total of 18 emerging modes are observed at 38 GPa. Simultaneously, a decrease in relative intensity of the other modes is observed; these modes fully disappear at 38 GPa. In the experiment performed without using PTM [Fig. 3(a)], the same process happens at a higher pressure of 29.6 GPa but more gradually. Finally, in the experiment

TABLE III. Experimental (Exp.) and calculated (Calc.) crystal parameters for wolframite $P2/c$ phase of $FeWO_4$, $CoWO_4$, and $NiWO_4$.

	$FeWO_4$		$CoWO_4$		$NiWO_4$	
Cell parameters and Wyckoff positions	Exp.[17]	Calc.	Exp.[18]	Calc.	Exp.[18]	Calc.
a (Å)	4.753	4.7889	4.6698	4.5583	4.5992	4.5104
b (Å)	5.720	5.8278	5.6873	5.6183	5.6606	5.5842
c (Å)	4.968	5.0165	4.9515	4.8908	4.9068	4.8608
β (deg)	90.08	90.43	90.00	89.580	90.03	89.625
A cation site: $2f$ (1/2, y, 1/4)	0.6784	0.6698	0.6712	0.6587	0.6616	0.6542
W site: $2e$ (0, y, 1/4)	0.1808	0.1795	0.1773	0.1792	0.1786	0.1792
	0.2167	0.2134	0.2176	0.2217	0.2241	0.2245
O_1 site: $4g$ (x, y, z)	0.1017	0.1043	0.1080	0.1086	0.1105	0.1096
	0.5833	0.5650	0.9321	0.9269	0.9204	0.9263
	0.2583	0.2532	0.2540	0.26212	0.2644	0.2623
O_2 site: $4g$ (x, y, z)	0.3900	0.3742	0.3757	0.37847	0.3772	0.3802
	0.0900	0.1076	0.3939	0.40338	0.3953	0.4076

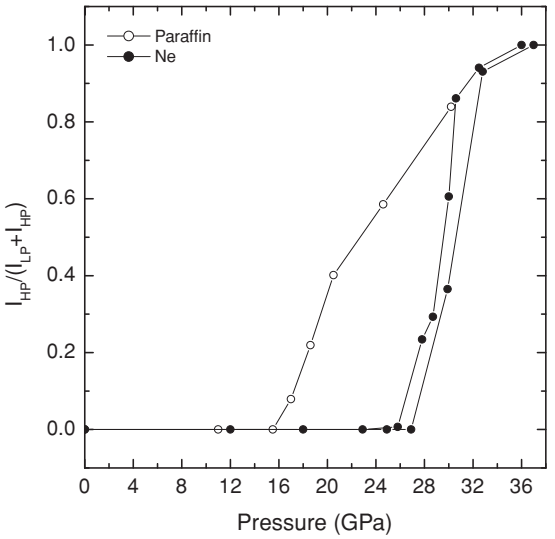

FIG. 7. Ratio between the intensity of the strongest peaks of wolframite (I_{LP}) and HP (I_{HP}) phases of $MgWO_4$. Solid symbols indicate Ne experiments, whereas empty ones are from the paraffin experiment.

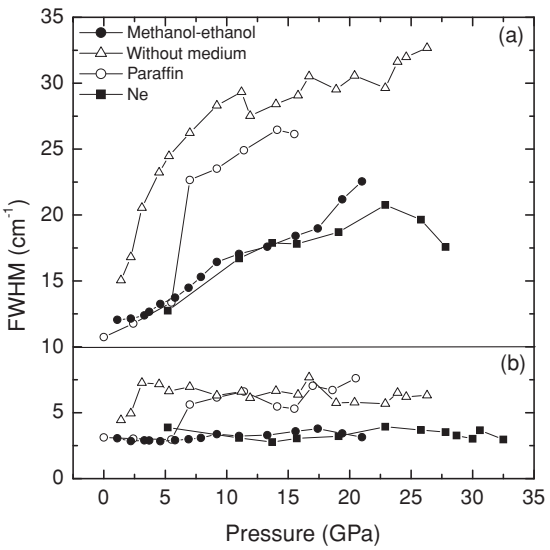

FIG. 8. FWHM of the highest (a) and lowest (b) frequency peaks of wolframite $MgWO_4$ at different pressures. Symbols indicate different experimental conditions.

with spectroscopic paraffin [Fig. 3(b)], the HP modes become evident as early as 17 GPa and the LP modes remain observable up to 30 GPa, the maximum pressure of the experiment. Phase coexistence is found in all three experiments, and the pressure range of coexistence depends upon the PTM used. To quantify the gradual transformation, we analyzed the effect of pressure on the intensities of distinctive modes of both phases and calculated the intensity ratio $I_{HP}/(I_{LP} + I_{HP})$.[34] In this equation, I_{HP} is the intensity of the highest-frequency mode of the HP phase, whereas I_{LP} is the highest-frequency mode of wolframite. Both modes are the strongest of each structure, and they do not overlap in the pressure range of coexistence, allowing a reasonable estimation of the HP/LP phase proportion. These modes are depicted by two arrows in Figs. 2, 3(a), and 3(b). The results are plotted in Fig. 7, where in experiments using Ne a steep increase of the intensity ratio can be seen, from 0 at 26 GPa (only LP phase) to 1 at 36 GPa (only HP phase). In contrast, in the experiment using paraffin, the changes are detected at 17 GPa, reaching the intensity ratio 0.8 at 30 GPa. This indicates that at 30 GPa domains of the LP phase are still present. From Fig. 5, it can be extrapolated that the intensity ratio would reach 1 around 36 GPa, as is the case when Ne was the PTM. These results, in combination with the appearance of the same bands after the phase transition in all experiments, indicate that the mechanism of the phase transition is the same for all experiments. However, the onset pressure depends upon the hydrostaticity of the PTM. The transition is detected at the lowest pressure when the experiment is performed with paraffin, suggesting that beyond 10 GPa paraffin becomes stiffer than the wolframites. A similar behavior was observed previously for $ZnWO_4$[6,8] indicating that nonhydrostatic conditions in wolframites accelerate the transition onset.

The effect of nonhydrostaticity on $MgWO_4$ becomes further visible from the analysis of the pressure dependence of the full width at half maximum (FWHM) for some Raman modes. In Fig. 8 we show the results for two modes of $MgWO_4$, the A_g mode at 916.8 cm^{-1} [Fig. 8(a)] and the B_g mode at 97.4 cm^{-1} [Fig. 8(b)], under four experimental conditions. It can be concluded that wolframites pressurized without any PTM suffer uniaxial stresses that are important even at LPs, as evidenced by the strong peak broadening. In the experiment using paraffin, we found a steep increase of the FWHM for both modes beyond 5 GPa. At this pressure, bands are as broad as they are without PTM, indicating that experimental conditions are far from quasihydrostaticity. On the other hand, in the experiments using Ne and methanol-ethanol, the Raman bands remain narrow up to 36 and 21 GPa (the maximum pressure reached), respectively. Therefore, uniaxial stresses are not noticeable in these experiments. This is consistent with no detected phase transition up to 21 GPa in the methanol-ethanol experiment. The methanol-ethanol mixture provides better quasihydrostatic conditions compared to paraffin.[22,35] Similar conclusions have been drawn recently from PXRD studies in the related material $BaWO_4$.[36] Therefore, all preceding facts suggest that nonhydrostaticity could play a key role on the acceleration of the phase transition in wolframites. These results explain why in previous PXRD experiments performed on $MgWO_4$ in silicone oil[6] the onset of the transition from wolframite to the HP phase occurs around 11 GPa lower compared to the Ne experiments of this study; i.e., the results obtained using silicone oil are similar to those obtained using paraffin because of the lack of good hydrostaticity of both PTM above 10 GPa. The use of ruby fluorescence to check hydrostaticity in DAC experiments is commonly accepted.[22] Therefore, to further check the nonhydrostaticity hypothesis, we also followed the FWHM of the fluorescent R_1 line of ruby in the experiments performed in Ne, as well as without PTM. The obtained results support the conclusions about nonhydrostaticity derived from the analysis of Raman modes in $MgWO_4$. The FWHM of the R_1 line is the same in both experiments up to 5 GPa (0.5 nm). Beyond this pressure, it

TABLE IV. Experimental and *ab initio* calculated Raman frequencies considering $P\bar{1}$ and $C2/c$ structures, as well as pressure coefficients for the HP phase of $MgWO_4$.

Ab initio $P\bar{1}$ at 30.5 GPa			*Ab initio* $C2/c$ at 38.4 GPa			Experiment at 30.6 GPa	
Mode	ω (cm^{-1})	$d\omega/dP$ ($cm^{-1}GPa^{-1}$)	Mode	ω (cm^{-1})	$d\omega/dP$ ($cm^{-1}GPa^{-1}$)	ω (cm^{-1})	$d\omega/dP$ ($cm^{-1}GPa^{-1}$)
A_g	124.3	0.40	B_g	177.9	0.24	166	0.60
A_g	155.6	0.00	A_g	217.5	0.00	185	2.01
A_g	193.0	0.01	B_g	220.2	0.38	210	1.52
A_g	235.5	0.82	A_g	271.0	0.71	239	0.71
A_g	291.9	0.93	B_g	295.5	0.71	276	2.18
A_g	300.7	0.47	A_g	377.9	1.59	345	1.62
A_g	343.2	0.59	B_g	391.0	1.14	383	1.89
A_g	367.3	2.45	A_g	394.7	3.39	393	1.09
A_g	457.0	1.62	B_g	423.4	2.88	420	2.02
A_g	474.6	2.52	A_g	490.2	2.85	441	2.46
A_g	475.8	2.55	B_g	528.3	2.2	531	2.75
A_g	551.7	3.56	B_g	609.9	2.53	542	0.88
A_g	619.5	3.34	B_g	647.2	2.60	609	0.62
A_g	650.0	2.53	A_g	717.3	2.18	700	2.91
A_g	805.4	3.46	A_g	834.9	1.95	724	2.63
A_g	815.8	2.84	B_g	877.6	2.21	801	2.63
A_g	939.6	2.96	A_g	918.7	2.70	833	3.26
A_g	1016.6	2.23	B_g	942.1	3.03	971	1.45

increases in both experiments but at a very different rate. In the experiment with no PTM it grows up to 2 nm at 31 GPa, whereas for the Ne experiment it is constrained to be smaller than 0.9 nm. This fact confirms that different stress distributions are present within the pressure chamber in different experiments.

To conclude this work, we comment on the structure of the HP phase of $MgWO_4$. Previous calculations and Raman experiments on $ZnWO_4$[8] and PXRD studies on $ZnWO_4$ and $MgWO_4$[6] proposed the following HP structural sequence: $P2/c \rightarrow P\bar{1} \rightarrow C2/c \rightarrow cmca$. However, the structure of the HP phase of wolframites is not fully determined yet. According to calculations, wolframite and a triclinic structure ($P\bar{1}$) are energetically competitive from 1 atm to 30 GPa.[6] A transition between both phases could be triggered by uniaxial stresses and would not involve any volume change. In addition, the PXRD pattern of the HP phase of $MgWO_4$ cannot be indexed with the monoclinic $C2/c$ structure and can be well explained considering the $P\bar{1}$ one. For better identification of the HP phase of $MgWO_4$, the experimental results are compared with the calculated Raman modes of the two HP phase candidates ($P\bar{1}$ and $C2/c$) in Table IV. According to Table IV, it seems reasonable to affirm that the HP phase of $MgWO_4$ better resembles the triclinic structure than the monoclinic ($C2/c$) one. In particular, the calculated low- and high-frequency modes well match the experimentally measured ones; they are within 5%. The same goes for the pressure coefficients. However, agreement is not so good for the modes of intermediate frequencies. In Fig. 9, we compare Raman spectra of the HP phases of Mg, Zn, and Cd wolframites with the Raman spectrum of the triclinic phase of $CuWO_4$ at ambient pressure. We also added ticks corresponding to the calculated modes for $C2/c$ and $P\bar{1}$ structures of $MgWO_4$. The

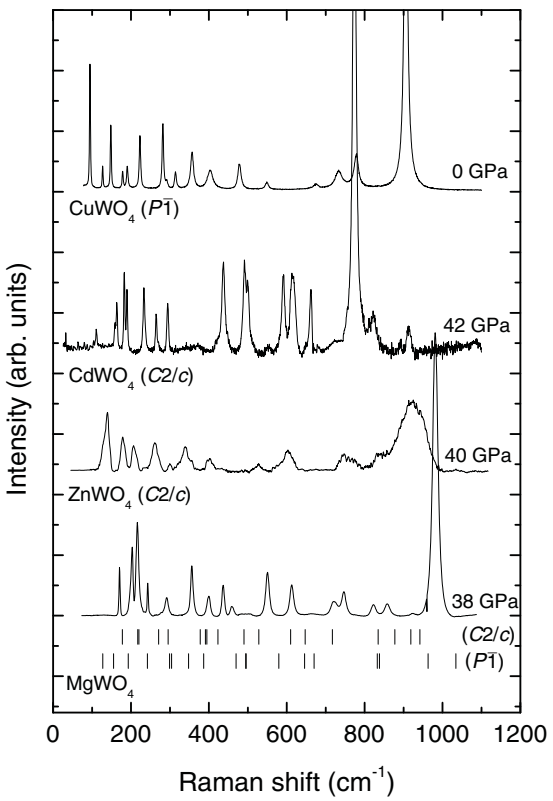

FIG. 9. Raman spectra of the HP phases of $MgWO_4$, $ZnWO_4$ (Ref. 8), and $CdWO_4$ (Ref. 9) wolframites around 40 GPa. The tips indicate the *ab initio* calculated modes considering the triclinic ($P\bar{1}$) and monoclinic β-fergusonite ($C2/c$) phases at 30.5 and 38.4 GPa, respectively. The Raman spectrum of triclinic $CuWO_4$ at ambient pressure (Ref. 10) is included for comparison.

Raman spectrum of HP-$MgWO_4$ shows more similarities with that of triclinic $CuWO_4$ than with those of monoclinic ($C2/c$) HP-$CdWO_4$ and HP-$ZnWO_4$. The only difference between the Raman spectrum of HP-$MgWO_4$ and that of $CuWO_4$ is the shifting of Raman modes toward higher frequencies because of compression in HP-$MgWO_4$. In both cases, there is a group of 12 modes at low frequencies plus three pairs of modes at high frequencies associated to internal vibrations of the WO_6 octahedra. These observations provide additional support to the hypothesis that the HP phase of $MgWO_4$ could have a triclinic structure. However, further structural studies are requested to fully confirm it.

V. CONCLUSION

We performed Raman experiments on $MgWO_4$ using four PTM with different hydrostaticity (Ne, methanol-ethanol, paraffin, and no medium). We detected a phase transition and determined the pressure dependence of the Raman modes of the LP and HP phases. We also observed that nonhydrostatic conditions strongly affect the phase transition onset and the range of pressures at which coexistence of HP and LP phases occurs. Moreover, we performed calculations that support our experimental conclusions and helped us with the mode assignment and the identification of the possible structure of the HP phase. We tentatively propose that the HP phase of $MgWO_4$ has a triclinic structure similar to that of $CuWO_4$. In addition, we reported Raman measurements in $MnWO_4$, $FeWO_4$, $CoWO_4$, and $NiWO_4$ at ambient pressure and provided calculations for these compounds at both ambient pressure and HP. A systematic comparison between theory and experiments is presented for the whole family of wolframites, and the effect of the divalent cation on the Raman frequencies is discussed.

ACKNOWLEDGMENTS

Research was financed by the Spanish Ministerio de Educación y Ciencia (MEC) under Grants No. MAT2010-21270-C04-01/02/04, and No. CSD-2007-00045. J. R.-F. thanks the MEC for support through the FPI program, as well as the SPP1236 central facility in Frankfurt for its use. F. J. M. acknowledges support from Vicerrectorado de Investigación y Desarrollo de la Universitat Politècnica de València (UPV) (Grant No. UPV2010-0096). A. M. and P. R.-H. acknowledge the supercomputer time provided by the Red Española de Supercomputación. A. F. appreciates support from the German Research Foundation (Grant No. FR2491/2-1).

*javier.ruiz-fuertes@uv.es.

[1] D. Errandonea and F. J. Manjon, Prog. Mater. Sci. **53**, 711 (2008), and references therein.
[2] J.-H. Zhao, T. Liu, S.-S. Guo, J. Guan, and X.-L. Wang, Opt. Express **18**, 18989 (2010).
[3] R. Lacomba-Perales, J. Ruiz-Fuertes, D. Errandonea, D. Martínez-García, and A. Segura, Eur. Phys. Lett. **83**, 37002 (2008).
[4] V. B. Mikhailik, H. Kraus, V. Kaputstyanyk, M. Panasyuk, Y. Prots, V. Tsybulskyi, and L. Vasylechko, J. Phys. Condens. Matter **20**, 365219 (2008).
[5] A. W. Sleight, Acta Cryst. B **28**, 2899 (1972).
[6] J. Ruiz-Fuertes, S. López-Moreno, D. Errandonea, J. Pellicer-Porres, R. Lacomba-Perales, A. Segura, P. Rodríguez-Hernández, A. Muñoz, A. H. Romero, and J. González, J. Appl. Phys. **107**, 083506 (2010).
[7] J. Macavei and H. Schulz, Z. Kristallogr. **207**, 193 (1993).
[8] D. Errandonea, F. J. Manjón, N. Garro, P. Rodríguez-Hernández, S. Radescu, A. Mújica, A. Muñoz, and C. Y. Tu, Phys. Rev. B **78**, 054116 (2008).
[9] R. Lacomba-Perales, D. Errandonea, D. Martínez-Gracía, P. Rodríguez-Hernández, S. Radescu, A. Mújica, A. Muñoz, J. C. Chervin, and A. Polian, Phys. Rev. B **79**, 094105 (2009).
[10] J. Ruiz-Fuertes, D. Errandonea, R. Lacomba-Perales, A. Segura, J. González, F. Rodríguez, F. J. Manjón, S. Ray, P. Rodríguez-Hernández, A. Muñoz, Zh. Zhu, and C. Y. Tu, Phys. Rev. B **81**, 224115 (2010).
[11] S. López-Moreno, A. H. Romero, P. Rodríguez-Hernández, and A. Muñoz, High Press. Res. **29**, 578 (2009).
[12] F. A. Danevich, D. M. Chernyak, A. M. Dubovik, B. V. Grinyov, S. Henry, H. Kraus, V. M. Kudovbenko, V. B. Mikhailik, L. L. Nagornaya, R. B. Podviyanuk, O. G. Polischuk, I. A. Tupitsyna, and Y. Y. Vostretsov, Nucl. Instrum. Methods Phys. Res. A **608**, 107 (2009).
[13] H. K. Mao, J. Xu, and P. M. Bell, J. Geophys. Res. **91**, 4673 (1986).
[14] A. Mujica, A. Rubio, A. Muñoz, and R. J. Needs, Rev. Mod. Phys. **75**, 863 (2003).
[15] P. E. Blöchl, Phys. Rev. B **50**, 17953 (1994).
[16] G. Kresse and D. Joubert, Phys. Rev. B **59**, 1758 (1999).
[17] G. Kresse and J. Hafner, Phys. Rev. B **47**, 558 (1993); **49**, 14251 (1994). Comput. Mater. Sci. **6**, 15 (1996); Phys. Rev. B **54**, 11169 (1996).
[18] J. P. Perdew, K. Burke, and M. Ernzerhof, Phys. Rev. Lett. **77**, 3865 (1996).
[19] H. J. Monkhorst and J. D. Pack, Phys. Rev. B **13**, 5188 (1976).
[20] S. L. Dudarev, G. A. Botton, S. Y. Savrasov, C. J. Humphreys, and A. P. Sutton, Phys. Rev. B **57**, 1505 (1998).
[21] K. Parlinski, Computer code PHONON. See [http://wolf.ifj.edu.pl/phonon].
[22] S. Klotz, J. C. Chervin, P. Munsch, and G. Le Marchand, J. Phys. D **42**, 075413 (2009).
[23] M. N. Iliev, M. M. Gospodinov, and A. P. Litvinchuk, Phys. Rev. B **80**, 212302 (2009).
[24] J. Ruiz-Fuertes, private communication, (2011).
[25] F. J. Manjón, D. Errandonea, N. Garro, J. Pellicer-Porres, P. Rodríguez-Hernández, S. Radescu, J. López-Solano, A. Mujica, and A. Muñoz, Phys. Rev. B **74**, 144111 (2006).
[26] C. Wilkinson and M. J. Sprague, Z. Kristallogr. **145**, 96 (1977).
[27] E. Garcia-Matres, N. Stüßer, M. Hofmann, and M. Reehuis, Eur. Phys. J. B **32**, 35 (2003).

[28]N. Hollman, Z. Hu, T. Willers, L. Bohaty, P. Becker, A. Tanaka, H. H. Hsieh, H. J. Lin, C. T. Chen, and L. H. Tjeng, e-print arXiv:1009.4338 (2010).
[29]C. Escobar, H. Cid-Dresdner, P. Kittl, and I. Duemler, Am. Mineral. **56**, 489 (1971).
[30]H. Weitzel, Z. Kristallogr. **144**, 238 (1976).
[31]L. Gracia, A. Beltrán, and D. Errandonea, Phys. Rev. B **80**, 094105 (2009).
[32]D. Errandonea, D. Santamaría-Perez, A. Vegas, J. Nuss, M. Jansen, P. Rodríguez-Hernandez, and A. Muñoz, Phys. Rev. B **77**, 094113 (2008).
[33]A. Kuzmin, A. Kalinko, and R. A. Evarestov, Cent. Eur. J. Phys. **9**, 502 (2011).
[34]D. Errandonea, R. Boehler, S. Japel, M. Mezouar, and L. R. Benedetti, Phys. Rev. B **73**, 092106 (2006).
[35]D. Errandonea, Y. Meng, M. Somayazulu, and D. Häusermann, Physica B **355**, 116 (2005).
[36]D. Errandonea, J. Pellicer-Porres, F. J. Manjón, A. Segura, Ch. Ferrer-Roca, R. S. Kumar, O. Tschauner, P. Rodríguez-Hernández, J. López-Solano, S. Radescu, A. Mújica, A. Muñoz, and G. Aquilanti, Phys. Rev. B **72**, 174106 (2005).